Bulletin of Earthquake Engineering (2019) 17:1667–1688
https://doi.org/10.1007/s10518-018-0510-x

ORIGINAL RESEARCH

Performance-based assessment of bridges with steel-SMA reinforced piers in a life-cycle context by numerical approach

Yue Zheng[1] · You Dong[2]

Received: 26 February 2018 / Accepted: 29 October 2018 / Published online: 7 November 2018

Abstract

Reconnaissance of structural damage under earthquakes has indicated that though current design philosophy can reduce structural collapse probability, it results in a significant reduction of functionality following earthquakes considering residual drift and numerous bridges had to be demolished. To protect bridges against earthquakes and reduce the residual drift, shape memory alloy (SMA) is studied and incorporated in the plastic hinge region of reinforced concrete (RC) piers to increase the resilience of bridges. The performance-based engineering (PBE) of SMA bar reinforced RC bridges considering residual drift ratio and maximum displacement is assessed by taking advantages of self-centering and energy dissipation features of SMA, specifically under extensively large seismic events. Additionally, the PBE is conducted within the lifetime of bridges considering the corresponding economic impacts. The proposed approach is illustrated within highway bridges with and without using SMA bars in the piers.

Keywords SMA bar reinforced pier · Residual drift · Probabilistic seismic demand · Performance-based engineering · Lifetime failure loss

1 Introduction

Highway bridges play an important role in the livelihood, welfare, and safety of any community and they could be subjected to natural hazards (e.g., earthquakes) during their service life. Based on the post-earthquake damage data, a large number of bridges with reinforced concrete (RC) piers encountered severe damage yet not collapse and had to be demolished due to large unrecoverable residual drift (Kawashima et al. 1998). Considering high repair cost associated with severely damaged bridge and increased importance of resilience-informed engineering, the high-performance seismic resistance

✉ You Dong
you.dong@polyu.edu.hk

Yue Zheng
yzheng@tongji.edu.cn

1 Department of Bridge Engineering, Tongji University, Shanghai, China

2 Department of Civil and Environmental Engineering, The Hong Kong Polytechnic University, Kowloon, Hung Hom, Hong Kong

systems with self-centering and energy dissipation capacity have been developed to mitigate the seismic loss of bridges under earthquake (Choi et al. 2005; Palermo and Pampanin 2008; Zhang et al. 2009; Padgett et al. 2010; Roh and Reinhorn 2010; Ozbulut et al. 2011; Dezfuli and Alam 2013; Fang et al. 2014, 2017; Wang et al. 2016; Markogiannaki et al. 2017; Mashal and Palermo 2017; Agalianos et al. 2017; Zheng et al. 2018; Wang and Zhu 2018). For instance, some studies have been conducted on the application of novel materials associated with self-centering properties (e.g., SMA). SMA, as a smart material, can recover the shape either by hearing or removal of the applied forces. By considering flag-shaped hysteretic behavior of SMA, SMA-bar can result in an effective self-centering mechanism. For instance, the SMA restrainers were developed to limit displacement between the superstructure and substructure of bridges (Wilde et al. 2000; DesRoches and Delemont 2002; DesRoches et al. 2003; Andrawes and DesRoches 2005; Johnson et al. 2008). Additionally, an isolation system with SMA-wire or SMA-cable-based bearing was investigated by Choi et al. (2005), Dezfuli and Alam (2016) and Zheng et al. (2018), among others. Though both the SMA restrainer and SMA-based bearing can prohibit the bridge from experiencing large displacement, seismic vulnerability of the piers could be increased for sustaining force transferring from superstructure to substructure. SMA could also be used within the piers of bridges. The seismic vulnerability of piers reinforced with SMA bars was investigated by some studies, such as Billah and Alam (2015), Shrestha and Hao (2016), among others. For instance, Saiidi and Wang (2006) designed two 1/4-scale spiral RC piers reinforced by SMA bars in the plastic hinge region. The results of shaking table test showed that the SMA-RC piers were able to recover nearly all the post-yield displacement. Additionally, high performance ductile systems using traditional materials have also been developed to provide dissipation and self-centering capability. For instance, precast elements, assembled through post-tensioning technique as a rocking system, were developed to guarantee an appreciable energy dissipation and desired self-centering capacity. All these novel systems aim to increase the safety of a structure against collapse, while simultaneously decrease the residual displacements.

As stated previously, the application of SMA within the bridge seismic mitigation process has been studied previously. For instance, SMA-cable/bar restrainer was used to replace the steel restrainer and was installed at in-span hinge or interface between the girder and abutment (Choi et al. 2005; Dezfuli and Alam 2014). Most of these studies emphasized on the seismic vulnerability of piers without considering performance of other structural critical components, such as bearings. Choi et al. (2004) stated that both piers and bearings can suffer severe damage under earthquakes and performance should be both considered in the seismic vulnerability process. Fragility of a bridge based only on the vulnerable pier may lead to a bias and cannot cover all the failure scenarios (Nielson and DesRoches 2004). To the best knowledge of the authors, few studies have investigated seismic fragility of bridges with piers reinforced by SMA at a system level (Dezfuli and Alam 2016; Zheng et al. 2018). A systematic approach to assess the seismic vulnerability of bridges with SMA bars considering seismic performance of different structural components is needed. In this paper, the whole bridge seismic vulnerability is assessed by considering the residual drift ratio and bearing displacement. Fragility curves of both novel bridge with SMA-RC piers and conventional bridge are computed and compared based on the seismic demand analysis under a large number of nonlinear dynamic time history analyses. The residual drift ratio of SMA-RC pier and displacement of bearing are taken as seismic demand for fragility assessment at the bridge system level, which has not been well addressed by previous studies.

An approach to structural assessment and design under hazard effects is needed with more emphasis on the performance rather than resistance. This has led to the recent development of performance-based engineering (PBE). The Pacific Earthquake Engineering Research Center (PEER) has developed performance-based seismic design and assessment approaches considering consequences including repair loss, downtime, and facilities, among others. PBE is rapidly becoming the benchmark approach for assessing and designing civil infrastructures subjected to hazards. PBE provides the ability to achieve more informative predication of structural performance considering the connection between the structural design objectives and the client's expected performance goals (Dong and Frangopol 2016b, 2017). Though the principles of PBE have been developed, studies on the assessment of structural system incorporating novel materials are scarce. In this paper, the PBE is applied to investigate structural performance considering the adoption of novel materials (e.g., SMA). The increase of initial cost associated with the novel structural system hampers the wide application of SMA within the hazard mitigation process. The long-term performance of implementing SMA within highway bridges should be assessed by considering the potential seismic hazard, structural seismic performance, investigated time interval, monetary discount rate, direct and indirect costs. The computational flowchart of the long-term PBE of civil infrastructures under seismic hazard is indicated in Fig. 1. In this paper, the life-cycle engineering is incorporated with PBE for the comparative assessment of novel and conventional bridges under seismic hazards. As the investigated SMA-RC piers are relatively new structural system, many aspects remain unknown and yet to be explored. To aid the application of these novel structural systems, numerical studies can be conducted firstly, which could shed some light upon the experimental behavior. Once the simulated behavior of such system is fully understood, the experimental study can be conducted to investigate its performance. To best knowledge of the authors, the performance-informed lifetime assessment of bridges using SMA as reinforcement has not been investigated by previous studies.

In this paper, the system-level vulnerability and long-term performance of SMA-RC bridge and conventional bridge are investigated and compared. The probabilities of the structural component and system being in different damage states are assessed within a systematic manner based on the fragility analysis. The economic indicator considering the long-term loss of the investigated bridges under different seismic events is computed. The proposed approach can aid the development and application of novel materials and systems within the civil engineering. In this paper, seismic performance of bridge piers reinforced by SMA bars is emphasized and the outcomes of the study could aid the design of bridges reinforced with SMA bars to mitigate the seismic loss.

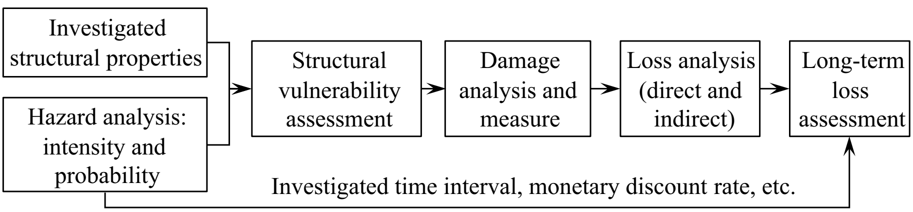

Fig. 1 Flowchart of the performance-based long-term engineering of civil infrastructures under seismic hazard

2 Seismic vulnerability analysis and experimental study

2.1 Analytical seismic vulnerability analysis

The seismic vulnerability of bridges is assessed using fragility curves, which quantify the probability of exceeding a certain damage state associated with critical components and system under a given hazard intensity. Seismic fragility analysis of bridges with traditional and novel materials has been studied by previous studies (Shinozuka et al. 2000; Padgett and DesRoches 2007; Dong et al. 2013; Dong and Frangopol 2015; Su et al. 2018; Zheng et al. 2018). Generally, fragility curves can be obtained using two approaches: empirical and analytical approach. Empirical fragility curves are based on bridge damage data from the previous earthquakes and experimental studies. In the absence of adequate empirical data and experimental studies, analytical methods can be used to develop fragility curves. Within the analytical approach, the structural demands and/or capacities used to evaluate failure probability are obtained based on numerical analysis. To obtain fragility curves of different structural components, it is necessary to specify the relevant demand and capacity models. The probabilistic seismic demand model (PSDM) is usually used to derive the seismic demands based on nonlinear time-history analysis. Given a suite of ground motions, the PSDM can be developed considering the relation between the engineering demand parameters (*EDP*s) (e.g., displacement, curvature ductility, drift ratio) to the ground motion intensity measures (*IM*s). The median value of *EDP* can be expressed as (Cornell et al. 2002)

$$EDP = a \cdot (IM)^b \tag{1}$$

where a and b are regression parameters derived from the analytical seismic responses. A 3D FE model can be established using OpenSees (McKenna et al. 2004) to assess the *EDP*. The standard deviation of ln (*EDP*) under given *IM* can also be assessed.

Given the seismic demand and capacity, the fragility curves can be quantified. The damage states are usually discrete and quantified by the designated thresholds of the Damage Index (*DI*) to define different Limit States (*LS*s). If the ground motion intensity *IM* is designated, the fragility curves can be calculated as

$$\mathrm{P}\left[DI \geq LS_i|IM\right] = 1 - \int_0^{LS_i} \frac{1}{\sqrt{2\pi} \cdot \xi_{EDP|IM} \cdot edp} \cdot e^{-\frac{\left[\ln(edp) - \ln\left(a \cdot IM^b\right)\right]^2}{2(\xi_{EDP|IM})^2}} d(edp) \tag{2}$$

where LS_i represents the ith *LS* and $\xi_{EDP|IM}$ is the standard deviation of the logarithmic distribution.

For bridges, piers and bearings are the critical components that are prone to seismic damage. Four Damage States (*DS*s) namely slight, moderate, extensive, and collapse were proposed by HAZUS (2003). The four *DSs* in terms of different *DI*s (e.g., sectional ductility, displacement ductility, residual drift ratio) can be quantified. According to the definitions presented by Berry and Eberhard (2003), slight *DS* represents minor cracking or spalling occurs at the pier and other three *DS*s are related to the yielding of longitudinal reinforcement and plastic hinge deformation. Choi et al. (2004) indicated that when the sectional ductility is larger than or equal to 1 yet smaller than 2, the RC pier only experiences slight damage (i.e., $DS=1$). When the maximal sectional ductility is larger than or equal to 2 yet smaller than 4, the pier would result in moderate *DS* (i.e., $DS=2$). When the sectional ductility is larger than or equal to 4 yet smaller than 7, the pier suffers extensive damage (i.e., $DS=3$). With respect to bearings, displacement and shear strain can be used as the *DIs*. More detailed information regarding damage states and other structural components can be found in Choi et al. (2004) and Zheng et al. (2018).

The damage states of the pier by considering residual displacement are illustrated herein. Based on Billah and Alam (2015), if the residual drift ratio (%) of RC pier is not larger than 0.25, the RC pier only experiences slight damage (i.e., $DS=1$). When the residual drift ratio (%) is larger than or equal to 0.25 yet smaller than 0.75, the pier would result in moderate *DS* (i.e., $DS=2$). Given the residual drift ratio (%) is larger than or equal to 0.75 yet smaller than 1.0, the pier suffers extensive damage (i.e., $DS=3$). Once the residual drift ratio (%) is larger than 1.0, the pier would collapse (i.e., $DS=4$). Given the seismic demand and capacity, the fragility curves and the probability of exceeding a certain *DS* can be obtained using Eq. (2). Consequently, the probability of being in a damage state i can be computed by the difference between the probabilities of exceedance of damage states i and $i+1$. Due to a critical lack of literature and experimental data on residual damage measures, tentative values based on experimental investigation of O'Brien et al. (2007) and Billah and Alam (2015) were selected to illustrate the proposed methodology in this paper. Further experimental studies are needed to verify the damage threshold values associated with different damage states.

Fragility curve of a bridge system can be developed considering the relationship among vulnerable components and assessing structural performance as a system. Previous studies suggest that system fragility can be determined by considering the functionality of bridges using a joint probabilistic seismic demand model of different vulnerable components (Shinozuka et al. 2000). Zhang and Huo (2009) proposed a composite *DS* to compute the system-level seismic behavior of bridges by using weighting factors considering the importance of different components within a bridge perceived by a decision maker. The system-level fragility curves can also be determined by assuming the failure modes. For instance, if a bridge is assumed to a serial system, the lower bound is the maximum component fragility and the upper bound is a combination of the component fragilities. Then, the bounds for a serial bridge system are

$$\max_{k=1}^{m} \left[P(F_k)\right] \leq P(F_{\text{sys}}) \leq 1 - \prod_{k=1}^{m} \left[1 - P(F_k)\right] \tag{3}$$

where m is number of vulnerable components; $P(F_k)$ is the probability failure of the kth component; $P(F_{sys})$ is the failure probability of the bridge system; and Π is the product operator. As indicated in Eq. (3), the lower bound refers to the case associated with complete correlation, while the upper bound assumes no correlation among the components. On the other hand, if a bridge is assumed as a parallel system, the damage state at the system-level will be achieved only if all the considered components reach the damage state. In reality, a bridge is neither a serial nor a parallel system. The seismic responses of the vulnerable components depend on the damage condition of all the components. Given the failure modes at the system level, the upper and lower bounds of the system fragility can be determined based on the first-order/second-order reliability theory.

2.2 Experimental studies on seismic performance of SMA and SMA reinforced piers

Using numerical method, the seismic vulnerability of the investigated structural component and system can be obtained analytically. It is of vital importance to verify the accuracy of the numeral simulation results. To address this aspect, some experimental tests were conducted on the SMA bars and SMA-bar reinforced piers (Fang et al. 2014, 2017). As depicted in Fig. 2, the numerical results match well within the experimental results for the SMA-bar. With respect to the SMA-bar reinforced pier, Saiidi et al. (2009) have conducted experimental study under pseudo-static test. A total of 8 longitudinal SMA bars were arranged evenly in a circular pattern at the plastic hinge region of the pier. The rest part of the pier is reinforced by steel with a yield stress of 472 MPa. The loading begins with one complete cycle in the push-and-pull direction to 0.25% drift ratio. More detailed information could be found in Saiidi et al. (2009). The numerical analysis of the SMA piers is conducted in this study. The associated results are compared with experimental results obtained from Saiidi et al. (2009). The test and numerical results of shear force verse displacement of the pier at the loading point are shown in Fig. 3a, b, respectively. The numerical results match well with the test result. The strain verse stress of the SMA bar is shown in Fig. 3c. Thus, the relevant results can verify the feasibility and accuracy of the numerical models used in this study.

3 Case study: fragility analysis of bridges with SMA bars reinforced piers

3.1 Bridge description

A novel bridge with SMA bar reinforced RC piers is selected to conduct seismic vulnerability assessment. The investigated bridge is a continuous RC bridge with two equal spans (i.e., 20 + 20 m). The configuration of the box girder, pier, and abutment is shown in Fig. 4. The height and width of the RC two-box girder are 1.2 and 12.5 m, respectively. The clear height of the SMA bar reinforced RC pier is 7.0 m, and the cross section of the RC pier is 0.9 m × 0.9 m. The total amount of concrete used in the bridges is 2061 m^3. To gain resilient capacity against intensive earthquakes, the SMA bars are arranged in the plastic hinge regions of the piers. The length of plastic hinge proposed by Paulay and Priestley (1992) is used (Saiidi and Wang 2006; Alam et al. 2008)

$$L_p = 0.08L + 0.002 d_b f_y \tag{4}$$

where L is the length of the member in mm; d_b is the diameter of SMA bar (mm); and f_y is the "yield strength" (i.e., phase transformation from austenite to martensite) of SMA

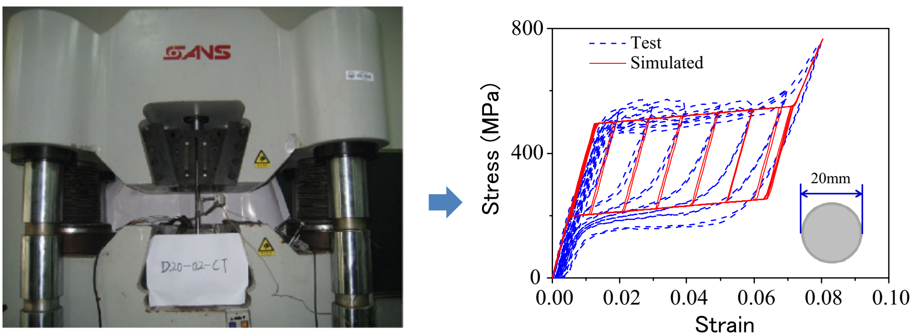

Fig. 2 Comparison results between the test and the numerical prediction of SMA bar

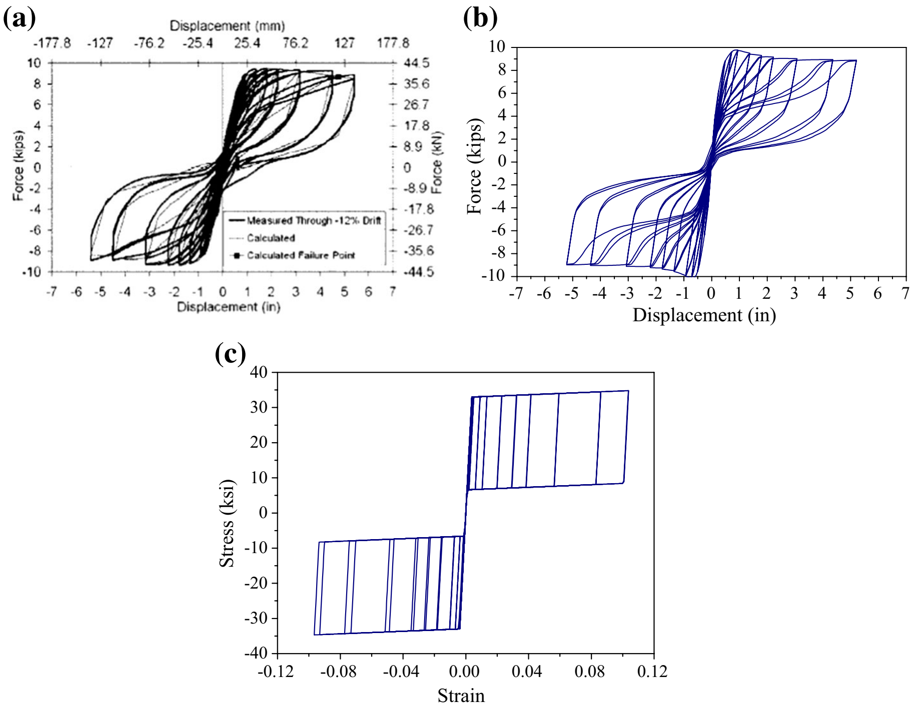

Fig. 3 Comparison of the numerical simulation and test results: **a** test results (adapted from Saiidi et al. 2009), **b** the authors' simulation results, and **c** strain verse stress of the SMA bar

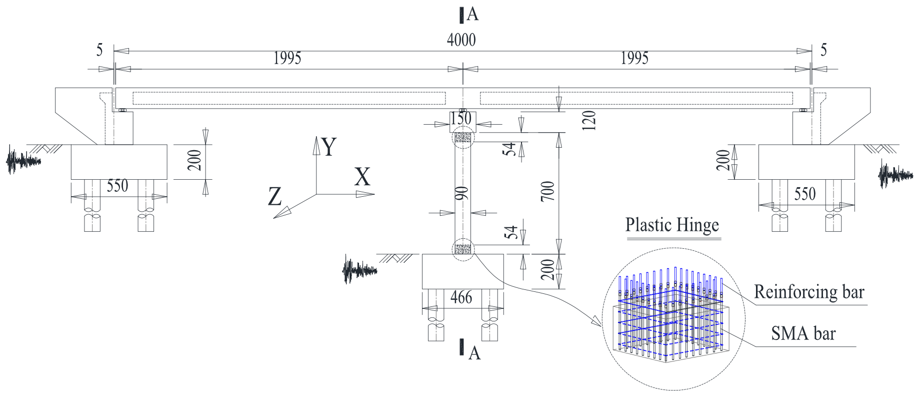

Fig. 4 Configuration for the continuous SMA bar reinforced RC bridge (unit: cm)

bar in MPa. The SMA bar with diameter of 30 mm is selected and arranged in the plastic hinge regions. In this study, the "yield strength" of the SMA bar is higher than that of conventional bar. The elastic modulus of the SMA bar (i.e., 58.8 GPa) is much lower than that of the conventional bar (i.e., 200 GPa). For the given material information, the length of the plastic hinge is 540 mm based on Eq. (4). The conventional reinforcing bars are used in other regions of the piers as the longitudinal reinforcement with diameter of 32 mm. The longitudinal reinforcement ratios of the SMA bar and conventional reinforcing bar are 2.79% and 3.18%, respectively. The transverse reinforcement ratio along the SMA bar reinforced RC pier is 0.25%. A total of 1030.5 m^3 concrete was used to build the individual bridge. The steel used for the conventional bridge was 91.9 tons while the steel for the novel bridge was 91.4 tons. The SMA bar of 0.41 tons was used to reinforce the pier in the plastic hinge region to improve its resilient capacity under earthquakes. The total construction cost of the conventional and novel bridges including bearings and abutments were 4.539 and 4.735 million CNY, respectively. By using SMA bar in bridge pier, the construction cost increases by 4.32%. Generally, the initial cost of the investigated novel bridges using SMA depends on many factors, such as material cost, labor cost, fabrication cost, among others. Given more information, the cost could be easily updated within this paper.

Figure 5 shows the bending moment versus curvature responses of the steel-RC and SMA-RC sections at the plastic hinge region using OpenSees. As indicated, before yielding the section reinforced by SMA has lower stiffness than that of the section reinforced by steel as the SMA bar has a smaller modulus of elasticity compared with steel bar. The bending moment capacities of SMA-RC and steel-RC sections are 3406.7 kN m and 3277.1 kN m, respectively. The material properties of concrete, SMA, and steel bar are summarized in Table 1.

3.2 Finite element modeling

The analytical 3D nonlinear FE models of both the conventional and novel bridges were established using OpenSees (McKenna et al. 2004) and the nonlinear time history analyses were conducted to develop fragility curves. The schematic FE model of the continuous RC bridge is shown in Fig. 6a. The RC box girder is model using elastic beam-column element. The conventional expansion bearings are placed on the top of abutments and two conventional fixed bearings are placed on top of bent cap. The constitutive performance of the expansion bearing is assumed as an elastic–plastic model. The yielding strength is computed as the product of the frictional coefficient (μ) and normal force (N) acting on the bearing. The initial elastic stiffness per millimeter (k_e) and frictional coefficient are 123.0 kN mm^{-1} and 0.2, respectively (Mander et al. 1996). The SMA-RC pier is modeled using the displacement-based nonlinear fiber elements to account for nonlinear characteristics. The constitutive behavior of the regular steel is modelled using a uniaxial material hysteretic model. The yielding strain of regular steel

Fig. 5 Moment and curvature relationship of steel-RC and SMA bar reinforced RC sections

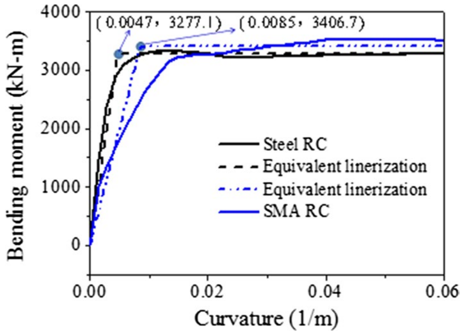

Table 1 Material properties of SMA-RC and steel-RC bridges

Material	Property	Value
Concrete	Compressive strength (MPa) at 28 days	30.0
	Strain at peak stress (%)	0.2
SMA	Elastic modulus (GPa)	58.8
	Austenite-to-martensite starting stress (MPa)	460.0
	Austenite-to-martensite finishing stress (MPa)	523.7
	Martensite-to-austenite starting stress (MPa)	366.8
	Martensite-to-austenite finishing stress (MPa)	302.8
Steel	Elastic modulus (GPa)	200.0
	Yield stress (MPa)	330.0
	Ultimate stress (MPa)	455.0
	Ultimate strain (%)	9.0

is 0.0017 and the corresponding strength is 330.0 MPa. The ultimate strain of the regular steel is 0.09 and the corresponding strength is 455.0 MPa. The SMA bar is modeled based on the flag-shaped constitutive relationship developed by Tremblay et al. (2008). The first "yielding strain" of the SMA rebar is 0.0078 and the corresponding strength is 460.0 MPa. The strain and strength of SMA rebar at the final phase of austenite to martensite are 0.08 and 523.7 MPa, respectively. The strain and strength of SMA rebar at starting phase transformation from martensite to austenite are 0.072 and 366.8 MPa, respectively. The strain and strength of SMA rebar at finishing phase transformation from martensite to austenite are 0.0052 and 302.8 MPa, respectively. The uniaxial Kent-Scott-Park concrete model (Scott et al. 1982) is used to model the unconfined and confined concretes. The compressive strength and corresponding strain of unconfined concrete at 28 days are 30.0 MPa and 0.002, respectively. The spalling strain of unconfined concrete is 0.004 (Priestley et al. 1996). The compressive strength of confined concrete and the corresponding strain at 28 days are 39.0 MPa and 0.003, respectively. The ultimate crushing strain ε_{cu} of confined concrete can be calculated as (Paulay and Priestley 1992)

$$\varepsilon_{cu} = 0.004 + 1.4\rho_s f_{yh} \varepsilon_{sm} / f_c' \tag{5}$$

where ρ_s is the volumetric ratio of stirrup; f_{yh} is the yielding strength of transverse steel in MPa; ε_{sm} is the steel strain at maximum tensile stress; and f_c' is the compressive strength of concrete in MPa at 28 days.

The seat-type cantilever RC abutments with U-shaped wing walls are supported on the concrete piles. The abutments are modeled using elastic beam-pier elements with constraint stiffness considering wall- and pile-soil interactions. The initial passive stiffness of the abutment due to the embankment material is 28.70 kN mm^{-1} m^{-1} (Caltrans 2010). The contribution of piles is considered by using a lateral stiffness of 7.0 kN mm^{-1} pile^{-1} (Caltrans 2010). The vertical stiffness is 175.0 kN mm^{-1} pile^{-1} (Choi 2002). This results in a translational spring constant of 56.0 kN/mm and a rotational spring constant of 6.09 kN m rad^{-1}. A tri-linear model of the force–displacement relationship was adopted to simulate the longitudinal response of seat-type abutment (Maragakis et al. 1991; Caltrans 2010) as indicated in Fig. 6c. The tri-linear model consists of three segments: (1) a zero-stiffness segment to account for the expansion gap; (2) a realistic stiffness segment for the embankment fill response; and (3) a yielding

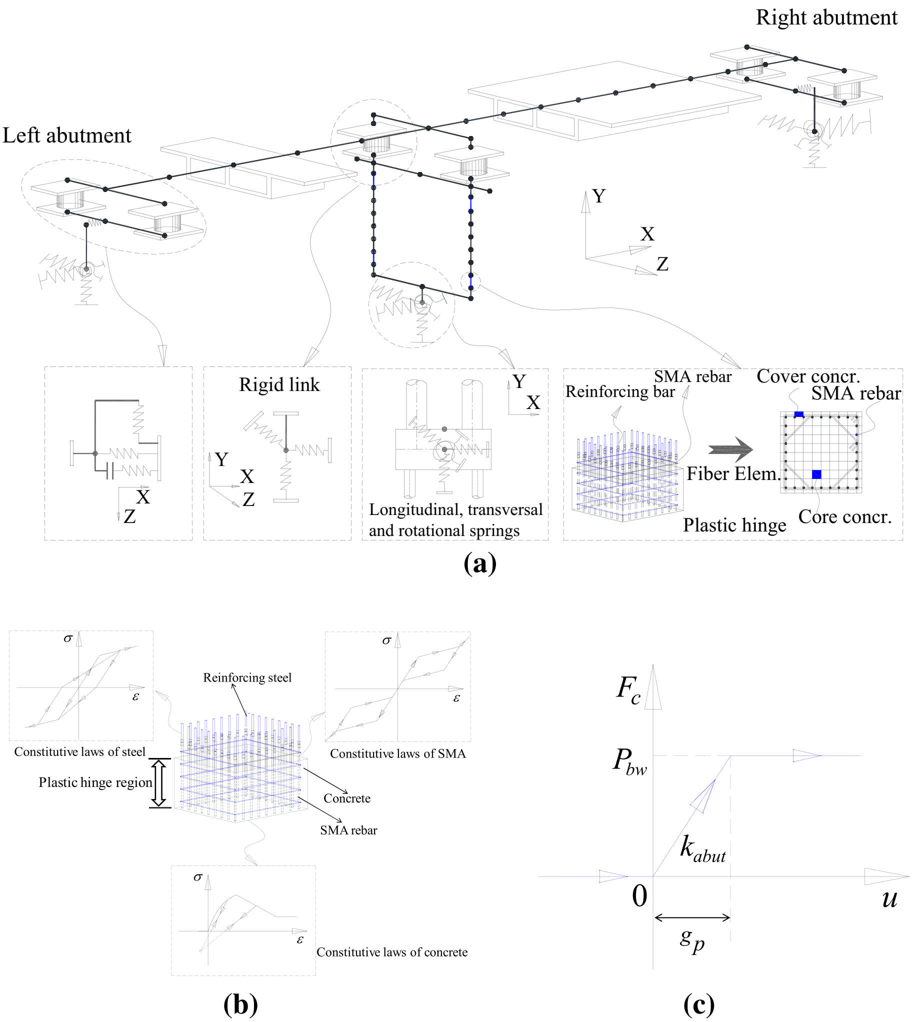

Fig. 6 **a** Nonlinear FE model of SMA-RC bridge; **b** configuration of plastic hinge of SMA-RC pier; and **c** hysteretic model of the seat-type cantilever abutment

stage segment with ultimate longitudinal force capacity P_{bw}. The stiffness of abutment k_{abut} and the passive pressure force resisting the moment at the abutment P_{bw} are computed as (Caltrans 2010)

$$k_{abut} = k_i \times w_{bw} \times \left(\frac{h_{bw}}{1.7}\right) \quad \text{(Unit: kN, m)} \tag{6}$$

$$P_{bw} = A_e \times 239 \times \left(\frac{h_{bw}}{1.7}\right) \quad \text{(Unit: kN, m)} \tag{7}$$

where w_{bw} and h_{bw} are projected width and height of the back wall associated with seat abutment and $A_e = h_{bw} \times w_{bw}$. For clarity, the tri-linear model of longitudinal response associated with seat-type abutment can be formulated by the following equations:

$$\begin{cases} F_c = 0 & u_i - u_j - g_p \leq 0 \\ F_c = k_{abut} \times (u_i - u_j - g_p) & 0 < u_i - u_j - g_p \leq P_{bw}/k_{abut} \\ F_c = P_{bw} & u_i - u_j - g_p > P_{bw}/k_{abut} \end{cases} \tag{8}$$

where F_c is the contact force; μ_i and μ_j are the displacements of pounding nodes *i* and *j*, respectively; and g_p is the gap distance.

3.3 Fragility curves

In order to conduct the nonlinear time-history analysis, a suite of 25 ground motion records were selected from the Pacific Earthquake Engineering Research Center Ground Motion Database (PEER 2013). The selected suite of records covers a broad range of peak ground acceleration (*PGA*) from 0.15 to 1.35 *g*. The fundamental periods of the conventional bridge and novel bridge are 0.277 s and 0.285 s, respectively. The period of the conventional bridge is shorter than that of the novel bridge.

PSDM is adopted to establish a correlation between the *EDP* and the *IM*. Though different *IM*s (e.g., *PGA*, peak ground velocity) can be selected, the *PGA* was recommended considering its efficiency, sufficiency, and computability in describing the ground motion (Mackie and Stojadinovic 2007; Padgett and DesRoches 2008). Herein, *PGA* is chosen as the *IM*. The seismic performance of the bearing and pier was investigated and median values corresponding to their appropriate *EDP*s were calculated based on Eq. (1). For the RC pier in the conventional bridge, taking maximum curvature ductility and residual drift ratio as the *EDPs*, the two sets of constants *a* and *b* are determined through regression analyses. The *a* and *b* with the conventional bridge considering the curvature ductility are 5.586 and 4.683, respectively. With respect to the residual drift ratio, they are 0.0023 and 12.14, respectively. Similarly, the values of *a* and *b* associated with piers of the novel bridge are 3.505 and 4.9 considering the curvature ductility and are 0.0001 and 18.99, based on the residual drift ratio, as indicated in Fig. 7a, b. The relevant regression parameters associated with bearings in both conventional and novel bridges can also be obtained. With respect to the investigated bridge, though some of the earthquake records could cause the collision between the girder and abutment, the maximum movement of abutment is 32 mm, which is much less than the threshold value of damage (HAZUS 1999).

4 Performance-based long-term seismic engineering

The PEER proposed a robust method for the PBE considering performance metrics that are relevant to decision making process of seismic risk mitigation (Ghobarah 2001; Porter 2003; Moehle and Deierlein 2004). The PBE could be conducted within four main analysis steps: hazard analysis, structural/nonstructural analysis, damage analysis, and loss analysis. The outcome of each step is characterized by four variables: Intensity Measure, Engineering Demand Parameter, Damage Measure, and Decision Variable. The process begins with definition of a ground motion Intensity Measure, which could

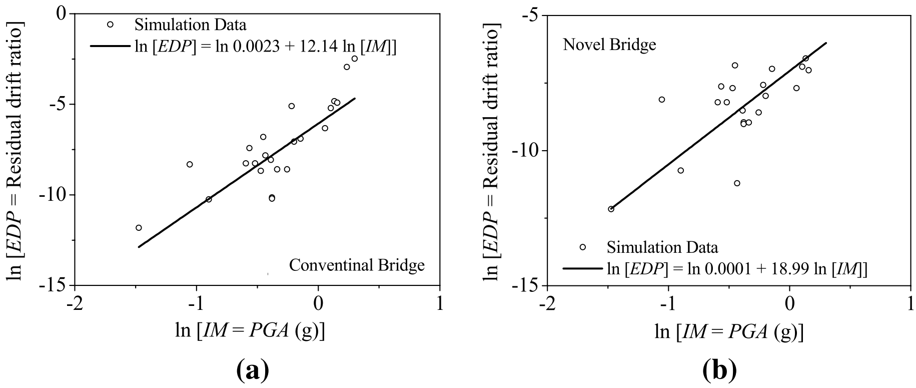

Fig. 7 Relationship of logarithmic *EDP* against *IM* of the **a** residual drift ratio of conventional bridge and **b** residual drift ratio of novel bridge

affect structural response. The next step is to determine Engineering Demand Parameters, which describe structural response in terms of displacement, accelerations, among others. Then, the Damage Measures are identified to assess the condition of structure and its components. Finally, the calculations of Decision Variables are conducted by translating the damage into quantities, such as repair costs, downtime, fatality, among others. The current design objectives aim to ensure the life safety, reduce damage under minor and moderate earthquakes, and prevent collapse in a major earthquake. The PBE can be used for comprehensive performance assessment and design of civil infrastructures under seismic hazard and aid the seismic mitigation process by considering different performance objectives in a more reliable and efficient way.

PBE of bridges under earthquakes is conducted in this section by considering different damage states to assess the economic impacts of bridges associated with both direct and indirect consequences, such as repair loss, human injuries, fatalities, property loss, etc. The direct consequence is usually related with the repair loss. The social metric includes time loss, rental loss, injuries, and fatalities, among others. Given the unit cost associated with downtime, the corresponding indirect loss of downtime can be computed (Dong and Frangopol 2016b; Frangopol et al. 2017). Parameters of quantifying consequences can be formulated based on information collected from material manufacturers, contractors, and government agencies. The repair loss, related to structural damage, is emphasized and other types of loss can also be incorporated within assessment process. The repair cost of a bridge can be calculated as a function of the percentage of total construction cost, which depends on local labor cost, availability of materials, and local construction practices. Under a given hazard event, the loss of bridge is computed as (based on Dong et al. 2013)

$$l = \sum_{DS} C_b \cdot (1 + \alpha_{ID|DS}) r_{cr|DS} \cdot P_{DS|H} \quad (9)$$

where C_b is the initial cost of a bridge, which is related with the amount of the materials used and the unit cost of the materials; $r_{cr|DS}$ is the repair cost ratio associated with a damage state DS; $P_{DS|H}$ is the conditional probability of being a damage state given IM; and $\alpha_{ID|DS}$ is the ratio between indirect and direct cost of the investigated damage state. The repair cost ratios with respect to slight, moderate, extensive, and collapse are 0.1, 0.3, 0.75, and 1.0, respectively (Mander 1999). Loss data from insurance companies can be used to derive an appropriate description of losses.

Quantifying the lifetime failure loss assessment can help the decision regarding the adoption of SMA within structural design and hazard mitigation procedure. Herein, long-term loss analysis is performed to support the hazard mitigation of using SMA within the investigated time interval. The flowchart of long-term performance-based engineering of structural systems using novel materials is indicated in Fig. 1. The investigated earthquake scenarios should be identified first. Then, the performance of the highway bridge with and without using SMA is assessed based on fragility curves, which have been addressed in the previous section. Given the probabilities of the bridges being in different damage states and the relevant consequence, the conditionally direct and indirect loss are quantified using Eq. (9). Subsequently, given the relevant parameters, the expected lifetime failure loss of the bridge within the investigated time interval t_{int} is (Dong and Frangopol 2016a)

$$E\left[Lt_i(t_{\mathrm{int}})\right] = \frac{\lambda_i \cdot E(l_i)}{\gamma} \cdot \left(1 - e^{-\gamma \cdot t_{\mathrm{int}}}\right) \tag{10}$$

where t_{int} is investigated time interval; l_j is the annual hazard loss; γ is the monetary discount rate; and λ_i is the mean rate of the Poisson model with respect to seismic event i. The long-term seismic loss should consider the possible earthquakes that can happen in the region. As the number of potential earthquakes may be extremely large, it is impractical to take the entire scenarios into consideration. Generally, several seismic events should be chosen to represent the seismic intensity. A hazard curve that quantifies the ground motion intensity versus occurrence frequency can be identified based on the USGS national seismic hazard map (USGS 2017). The points along the hazard curve refer to the seismic scenarios associated with different frequencies and intensities (e.g., *PGA*s). In this paper, ten seismic scenarios are selected and the expected long-term loss with respect to all the investigated scenarios is computed. The ten selected events are 10 (*E*1), 40 (*E*2), 72 (*E*3), 125 (*E*4), 225 (*E*5), 475 (*E*6), 975 (*E*7), 1500 (*E*8), 2475 (*E*9), and 5000-year (*E*10) return periods seismic intensities. The design event (i.e., *DE*) is regarded as the 10/50-year event associated with the 475-year return period. The maximum considered earthquake (*MCE*) usually refers to the 2/50-year event (2% in 50 years) and is related with the 2475-year return period. Given the location, the *PGA* associated with the ten seismic events can be predicted.

5 Results and discussion

5.1 Comparative seismic vulnerabilities of conventional and SMA-RC bridges

For conventional RC bridges, ductility of pier and bearing displacement are usually chosen as *EDPs* for seismic vulnerability assessment (Shinozuka et al. 2000; Choi et al. 2004). The novel bridge, incorporating smart material with excellent capacities of deformation recovery and energy dissipation, can experience large deformation during earthquakes, which does not mean that it will be damaged severely. In this regard, the residual drift ratio should be adopted as *EDP* for evaluating vulnerability of novel bridges besides deformation ductility. The fragility curves of conventional and novel bridges at the system level are indicated in this section. The failure mode in Eq. (3) is used for the system level fragility analysis and the expected value with the lower and upper bounds is adopted (Dong et al.

2013; Zheng et al. 2018). Given more information, other failure modes can also be used to assess the system-level fragility. In order to compare the fragility curves by using different *EDP*s, the curvature ductility of pier and displacement of bearing are taken as the first set *EDP*. The fragility curves of conventional and novel bridges corresponding to the four *DS*s (i.e., slight, moderate, extensive, and collapse) are obtained. Figure 8a is associated with the extensive damage state for these two bridges by using the first set EDP. It is evident that when the *PGA* is less than 0.590 *g* at extensive *DS*, the exceeding probability of extensive *DS* of the novel bridge is slight greater than that of the conventional bridge. The similar trend can also be found at other *DS*s.

The residual drift ratio of pier and displacement of bearing are taken as the second set *EDP* for fragility analysis. The relevant fragility curves of the conventional and novel bridges with respect to the extensive damage are graphed in Fig. 8f. As indicated, when the *PGA* is less than 0.83 *g*, the damage probability of the novel bridge is a little greater than that of the conventional bridge. As the elastic modulus of SMA bar is smaller than that of steel bar, the stiffness of SMA-reinforced pier is smaller than that associated with the steel-reinforced pier. As a result, the SMA-reinforced RC pier experienced more deformation. When both steel and SMA are within the elastic range, more damage could happen within in concrete of SMA-RC bridge pier. This could explain the scenario that the damage probability of SMA-RC bridge is slightly larger than that of conventional bridge under low PGA level. As far as the *PGA* exceeds 0.83 *g*, the exceeding probability of the novel bridge is smaller compared with the conventional bridge. Generally, with respect to high PGA level, the pier would result in nonlinear behavior. Considering the super-elastic property of SMA, it can return to its original shape after the event. The re-centering capability of SMA makes the pier less vulnerable under higher PGA level. Additionally, the difference between these two bridges could increase with the increase of the *PGA*. As indicated in Fig. 8b, given $PGA = 1.0\ g$, the probabilities that the conventional bridge system experiencing extensive damage is 14.6% larger than that of the novel bridge. Thus, it is can be concluded that the effectiveness of damage mitigation of novel bridge is much better than the conventional bridge by considering residual drift ratio as *EDP* at relatively high *PGA* values.

The two sets of *EDPs* are both used in PSDM for establishing fragility curve of the bridges at four *DSs*. As indicated in Fig. 9, it can be found that at a given *DS*, the exceeding probability of the novel bridge using the first set *EDP* is a little smaller than that using second set of *EDP* at relatively lower *PGA* levels. Once the *PGA* exceeds a threshold, the damage probability of the novel bridge based on the first set of *EDP* is significantly higher than that using the second set. As a result, for the relatively high *PGA*, fragility analysis taken the curvature ductility as *EDP* provides a conservative result.

A given ground motion input is selected to indicate the displacement responses, depicted in Fig. 10a. As indicated, the maximum displacements of the conventional and novel bridges are 0.25 and 0.249 m, respectively. The curvature responses in the plastic hinge are shown in Fig. 10b, of which the absolute maximum values of conventional and novel bridges are 0.045 and 0.044 m^{-1}, respectively. The residual curvature of the conventional bridge is 0.012, which is remarkably greater than that of the novel bridge (i.e., 0.0003). Thus, though both bridge systems have a similar maximum curvature response, the residual curvatures of two bridge systems are significantly different. Accordingly, using different *EDP*s (e.g., residual displacement or curvature ductility), it can lead to different results. The novel bridge has a good self-centering capacity, which mainly contributes to the embedded SMA bars in the plastic hinge region. Figure 10c illustrates the seismic response of the regular steel and SMA rebar at the plastic hinge region. The regular steel and SMA rebar experiences similar maximum strain responses (i.e., −0.010 and −0.011).

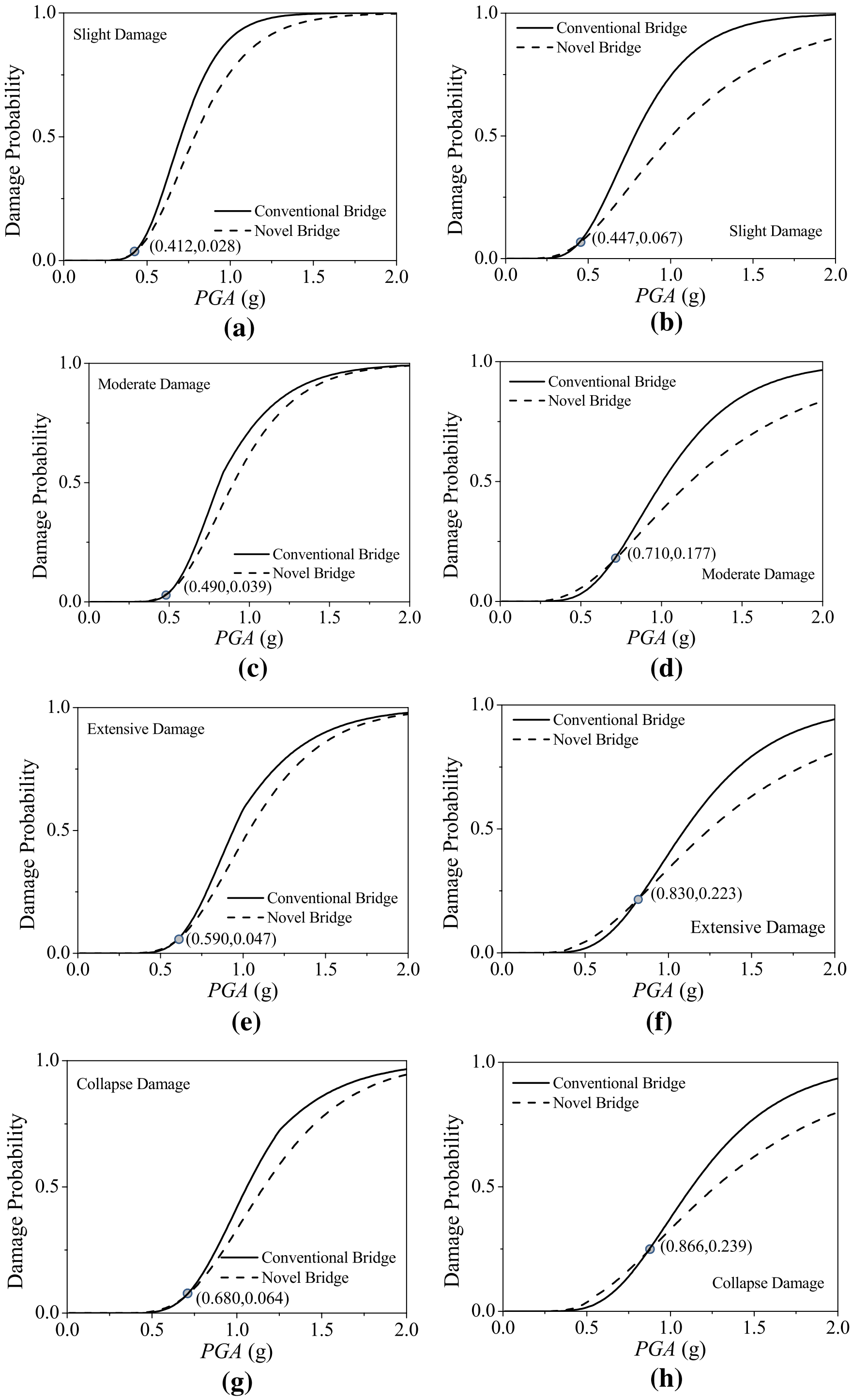

Fig. 8 Fragility curves of two bridge systems associated with four damage states quantified by first set of EDP (**a**, **c**, **e**, **g**) and second set of EDP (**b**, **d**, **f**, **h**)

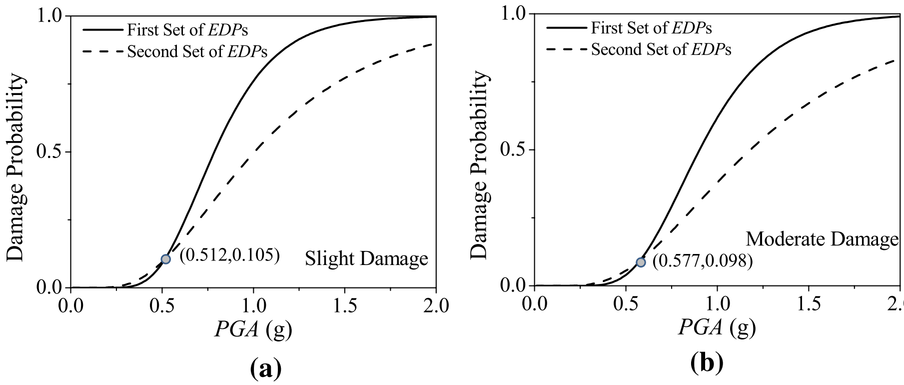

Fig. 9 Fragility curves of novel bridge associated with **a** slight damage and **b** moderate damage states

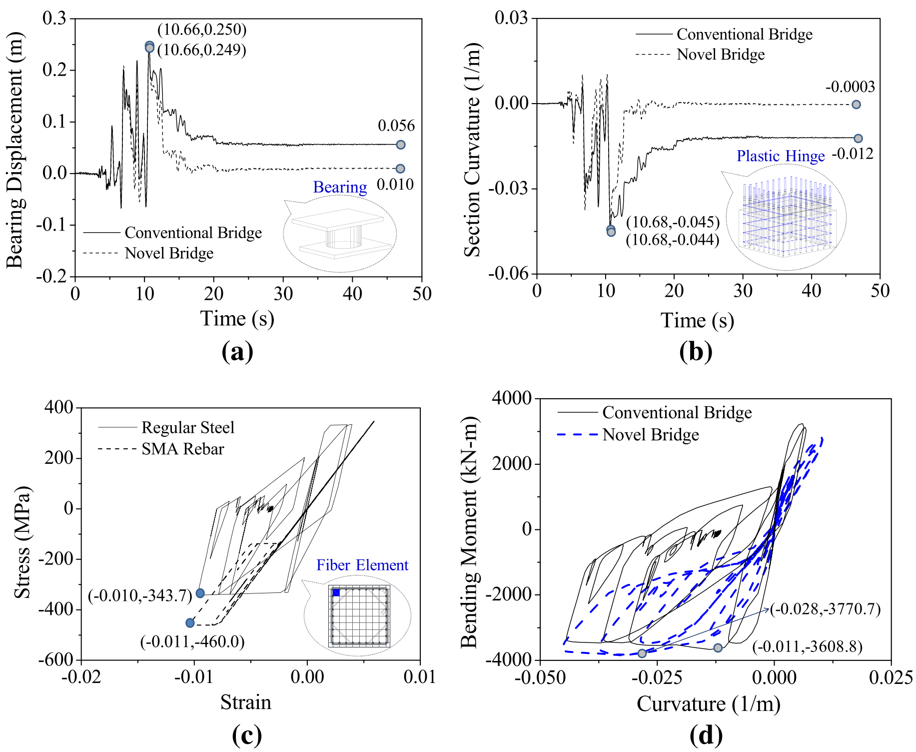

Fig. 10 Seismic responses of **a** bearing displacement, **b** sectional curvature, **c** strain versus stress of SMA and regular steels, and **d** bending moment versus of curvature of pier at plastic hinge under a given ground motion

The regular steel performs unrecoverable deformation while the SMA rebar can recover its original state. Figure 10d indicates that when the SMA-RC and RC piers experience curvatures of 0.028 and 0.011, both piers result in the yield state. The conclusion can be drawn that the SMA-RC pier is not only more flexible but also more resilient compared with the RC pier.

5.2 Performance-based long-term loss assessment

The performance-based seismic assessment of the investigated bridges is conducted herein based on the fragility curves and consequences associated with different damage states. As discussed previously, ten seismic events are selected and the loss with respect to all the investigated scenarios is computed. Hazard curve parameters for location of the investigated bridges are based on the United States Geological Survey (USGS 2017). The *PGA*s with return period of 10-, 40-, 72-, 125-, 225-, 475-, 975-, 1500-, 2475-, and 5000-year return periods are 0.0466, 0.1739, 0.2629, 0.3652, 0.4968, 0.6994, 0.9333, 1.0896, 1.2960, and 1.6307 *g*, respectively. Given the hazard scenarios (e.g., intensity and probability of occurrence), probabilities of the bridge being in different damage states, and the relevant repair cost ratio of different damage state, the direct repair loss is computed using Eq. (9). The 475- (i.e., design event, *DE*) and 2475-year (i.e., maximum considered event, *MCE*) return periods are firstly assessed. The repair loss of both conventional and novel bridges is shown in Fig. 11. The contribution of different damage states to the total expected loss is also indicated in this figure. As indicated, for the *MCE*, the complete/collapse damage state contributes dramatically to the total loss. The damage loss associated with complete damage states of conventional and novel bridges is approximately 96.9% and 91.4% of the total loss. For the *DE*, other damage states (i.e., slight, moderate, extensive) also contribute significantly to the total loss. For instance, for the novel bridge under the *DE*, the loss associated with complete damage is 55.4% of the total expected loss. Thus, with respect to the small and moderate seismic events, different levels of damage states should be considered within the PBE. Without considering the contribution of other damage states could lead to an underestimated loss. The total expected repair losses given the occurrence of the ten seismic events are shown in Fig. 12a. As indicated, the seismic loss increases with the hazard intensity. From the *E*7 to *E*10, the conventional bridge would result in a larger repair loss compared with the values of the conventional bridge.

Subsequently, given the occurrence model of the investigated seismic events and conditional loss, the expected total loss within the investigated time interval is computed using Eq. (10). This value provides a quantitative measure of the seismic performance of bridge systems under a given investigated time interval. The expected long-term

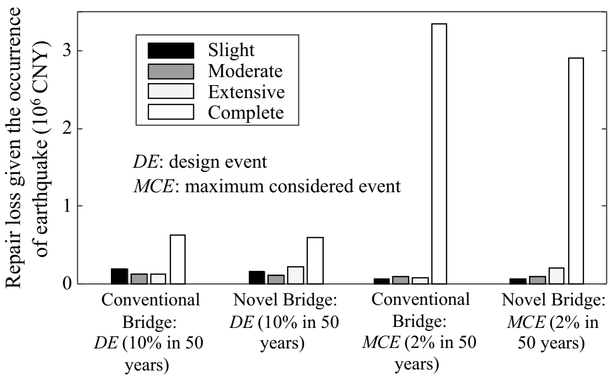

Fig. 11 The repair loss of the conventional and novel bridges given the occurrence of the design (*DE*) and maximum considered events (*MCE*)

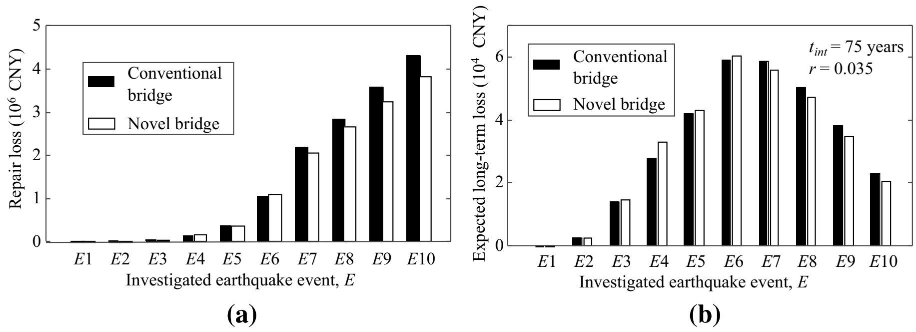

Fig. 12 **a** Repair loss of conventional and novel bridges given the occurrence of the ten events and **b** expected long-term loss under the ten events given $t_{int}=75$ years and $r=0.035$

seismic losses of the bridges under the ten events are shown in Fig. 12b. The monetary discount rate is 3.5% and the time interval is 75 years. As indicated, with respect to both the conventional and novel bridges, the maximum long-term loss among the ten events is *E6* (i.e., design event, *DE*). Thus, it is reasonable to take the 475-year return period event as the design event for both conventional and novel bridges. The expected long-term loss depends on not only the occurrence probability but also the hazard intensity. Additionally, the SMA bridge is more economically benefit under the extensively large and low probability of occurrence seismic events. As indicated, the SMA-RC bridge is associated with a larger loss compared with the conventional bridges from the *E*1 to *E*6. With respect to the *DE*, the expected long-term loss of the novel bridge is approximately 102.9% of that of the conventional bridge. For the *MCE*, expected long-term loss of the novel bridge is about 20,322 CNY, which is approximate 85% of that of conventional bridge. Though the *MCE* has a larger hazard intensity, the expected long-term loss of *DE* is much larger than that of the *MCE*, as the *DE* has a relatively larger occurrence probability during the investigated time interval. Then, given the return period of seismic event and expected long-term loss, the relationship between these two terms is fitted by using the exponential functions. As indicated in Fig. 13, the SMA bridge would result in a smaller long-term loss, given the return period of the seismic event is larger than approximate 540 years.

Fig. 13 Relationship between the return period of seismic events and the expected long-term loss

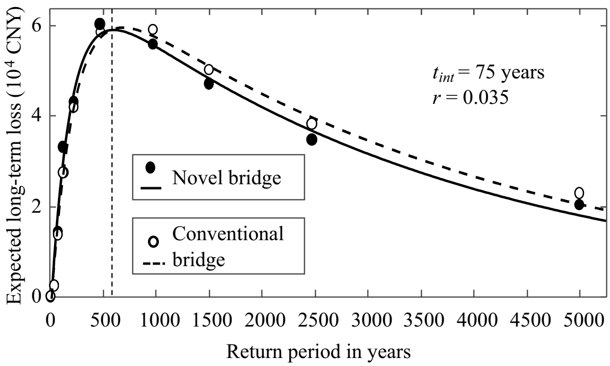

The effects of investigated time interval (t_{int}) and monetary discount rate (r) on the long-term loss are also assessed. As indicated in Fig. 14a, the expected loss increases as the time interval. As time increases, the expected loss trends to remain constant and investigated time interval would not have a significant effect. For the lifetime failure cost assessment, the monetary discount rate is usually between 2 and 7%. The smaller discount rate is usually used by the public sector and the larger discount rate is used by the private sector. Figure 14b shows the expected long-term loss for both the conventional and novel bridges under different monetary discount rates and the expected long-term loss decreases with the increase of the monetary discount rate. Compared with the investigated time interval, the monetary discount rate seems to have a larger effect on the expected long-term loss.

6 Conclusions

This study utilized performance-based engineering to conduct seismic fragility analysis and long-term loss assessment of conventional bridge and novel bridge with SMA-RC reinforced piers. Within the scope of this study, the PSDM was established in terms of two sets of *EDP*, of which one set *EDP* contains curvature ductility of pier and displacement of bearing and the other set of *EDPs* consists of residual drift ratio of pier and displacement of bearing. Then, fragility curves associated with the conventional and novel bridges at system level were obtained using nonlinear dynamic analysis. The comparative performance-based long-term performance of these two bridges were also assessed. The results are obtained based on the investigated specific bridge. Given more information, the proposed approach could be easily applied to other types of bridge. The following conclusions can be drawn.

(1) It was found that the SMA bar does not have a significant effect on the seismic demand by considering the peak displacement as a seismic demand parameter. By using SMA, the residual drift ratio can be reduced significantly, especially under extensively large earthquake events. Thus, the residual drift should be considered in the seismic vulnerability assessment of SMA-RC bridges.
(2) The residual drift ratio has a large effect on the seismic vulnerability of the bridges. If the residual drift ratio is used in PSDM, the damage probability of the novel bridge

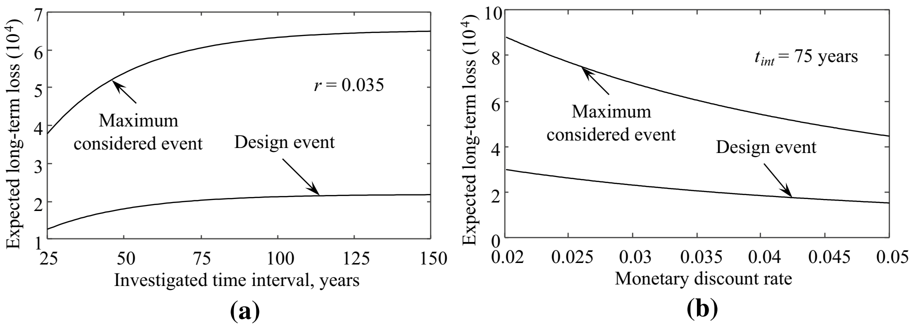

Fig. 14 Effects of **a** investigated time interval and **b** monetary discount rate on the expected long-term loss given the *DE* and *MCE*

reduced remarkably compared with the values using the maximum displacement as *EDP*. Taking the residual drift ratio as the *EDP*, the difference between the damage probabilities of these two bridges increases with the *PGA*. The opposition trend was found when taking the sectional ductility into consideration. Thus, for the relatively high PGA, fragility analysis taken the curvature ductility of pier as *EDP*s provides a conservative result.

(3) With respect to relatively small and moderate seismic event, without considering the contribution of other damage states (i.e., slight, moderate, extensive) could lead to an underestimated seismic loss. The complete/collapse damage state contributes dramatically to the total loss under the *MCE*.

(4) Given the largest expected long-term loss occurs with the design event (*DE*) for both bridge systems, it is reasonable to take the 475-year return period event as the design event. Additionally, the expected long-term loss depends not only on the return period (e.g., probability of occurrence) but also on the hazard intensity (e.g., value of *PGA*).

(5) By using SMA bars, the cost of the bridge increased by approximately 4%. The benefit of using SMA bars depends on the investigated hazard intensities, monetary discount rate, and investigated time interval. The SMA would result in a larger benefit for the bridges located in the seismic prone area. For instance, the expected long-term loss of using SMA under *MCE* is approximate 85% of that with respect to the conventional bridge, given the investigated time interval of 75 years and a monetary discount rate of 3.5%.

(6) In this paper, the life-cycle engineering is incorporated with performance-based engineering for the comparative assessment of novel and conventional bridges under seismic hazards. Experimental studies will be conducted in the future studies to verify the numerical simulation results and benefit of the proposed novel bridges reinforced by SMA bars. The proposed approach can be used within the design, assessment, and management of highway bridges under seismic hazards to prompt the development and application of novel materials and structural systems and enhance both the resilience and sustainability of the community.

Acknowledgements The study has been supported by The Hong Kong Polytechnic University under Start-Up Fund Number 1-ZE7Q, the Project of CNERC Fund Number 1-BBYU, and the Natural Science Foundation of the Shanghai Pujiang Program under Grant Number 16PJ1409600 are gratefully acknowledged. The opinions and conclusions presented in this paper are those of the authors and do not necessarily reflect the views of the sponsoring organizations.

References

Agalianos A, Psychari A, Vassiliou M, Stojadinovic B, Anastasopoulos I (2017) Comparative assessment of two rocking isolation techniques for a motorway overpass bridge. Front Built Environ. https://doi.org/10.3389/fbuil.2017.00047

Alam MS, Youssef MA, Nehdi M (2008) Analytical prediction of the seismic behavior of super-elastic shape memory reinforced concrete elements. Eng Struct 30:3399–3411

Andrawes B, DesRoches R (2005) Unseating prevention for multiple frame bridges using super-elastic devices. Smart Mater Struct 14:60–67

Berry M, Eberhard M (2003) Performance models for flexural damage in reinforced concrete columns. Report PEER 2003/18, PEER, University of California, Berkeley

Billah MAHM, Alam MS (2015) Seismic fragility assessment of concrete bridge pier reinforced with super-elastic shape memory alloy. Earthq Spectra 311:515–1541

California Department of Transportation (CLATRANS) (2010) Seismic design criteria, version 1.6, Sacramento, CA
Choi E (2002) Seismic analysis and retrofit of mid-America bridges. Ph.D. thesis, Georgia Institute of Technology
Choi E, DesRoches R, Nielson BG (2004) Seismic fragility of typical bridges in moderate seismic zones. Eng Struct 26:187–199
Choi E, Nam T, Cho BS (2005) A new concept of isolation bearings for highway steel bridges using shape memory alloys. Can J Civ Eng 32:957–967
Cornell AC, Jalayer F, Hamburger RO (2002) Probabilistic basis for 2000 SAC federal emergency management agency steel moment frame guidelines. J Struct Eng 128:526–532
DesRoches R, Delemont M (2002) Seismic retrofit of simply supported bridge using shape memory alloys. Eng Struct 24:325–332
DesRoches R, Pfeifer T, Leon RT, Lam T (2003) Full-scale tests of seismic cable restrainer retrofits for simply supported bridges. J Bridge Eng 8:191–198
Dezfuli FH, Alam MS (2013) Shape memory alloy wire-based smart natural rubber bearing. Smart Mater Struct 22(4):045013
Dezfuli FH, Alam MS (2014) Performance-based assessment and design of FRP-based high damping rubber bearing incorporated with shape memory alloy wires. Eng Struct 61:166–183
Dezfuli FH, Alam MS (2016) Seismic vulnerability assessment of a steel girder highway bridge equipped with different SMA wire-based smart elastomeric isolators. Smart Mater Struct 25:1–16
Dong Y, Frangopol DM (2015) Risk and resilience assessment of bridges under main shock and aftershocks incorporating uncertainties. Eng Struct 83:198–208
Dong Y, Frangopol DM (2016a) Time-dependent multi-hazard life-cycle assessment of bridges considering climate change. ASCE J Perform Constr Facil 30(5):301–312
Dong Y, Frangopol DM (2016b) Performance-based seismic assessment of conventional and base-isolated steel buildings including environmental impact and resilience. Earth Eng Struct Dyn 45:739–756
Dong Y, Frangopol DM (2017) Probabilistic life-cycle cost-benefit analysis of portfolios of buildings under flood hazard. Eng Struct 142:290–299
Dong Y, Frangopol DM, Saydam D (2013) Time-variant sustainability assessment of seismically vulnerable bridges subjected to multiple hazards. Earthq Eng Struct Dyn 42:1451–1467
Fang C, Yam MC, Lam AC, Xie L (2014) Cyclic performance of extended end-plate connections equipped with shape memory alloy bolts. J Constr Steel Res 94:122–136
Fang C, Wang W, He C, Chen Y (2017) Self-centring behaviour of steel and steel-concrete composite connections equipped with NiTi SMA bolts. Eng Struct 150:390–408
Frangopol DM, Dong Y, Sabatino S (2017) Bridge life-cycle performance and cost: analysis, prediction, optimization and decision making. Struct Infrastruct Eng 13:1239–1257
Ghobarah A (2001) Performance-based design in earthquake engineering: state of development. Eng Struct 23(8):878–884
HAZUS (2003) Multi-hazard loss estimation methodology earthquake model. Technical manual. Department of Homeland Security Emergency Preparedness and Response Directorate, FEMA Mitigation Division, Washington, DC
HAZUS99-SR2 (1999) Technical manual. National Institute of Building Sciences (NIBS) and Federal Emergency Management Agency, Washington, DC
Johnson R, Padgett JE, Maragakis ME, DesRoches R, Saiidi M (2008) Large scale testing of nitinol shape memory alloy devices for retrofitting of bridges. Smart Mater Struct 25:1–10
Kawashima K, MacRae G, Hoshikuma J, Nagaya K (1998) Residual displacement response spectrum. J Struct Eng 124:523–530
Mackie KR, Stojadinovic B (2007) Performance-based seismic bridge design for damage and loss limit states. Earthq Eng Struct Dyn 36:1953–1971
Mander JB (1999) Fragility curve development for assessing the seismic vulnerability of highway bridges. Technical Report, University at Buffalo, State University of New York
Mander JB, Kim DK, Chen SS, Permus GJ (1996) Response of steel bridge bearings to the reverse cyclic loading. Technical Report NCEER-96-0014
Maragakis E, Douglas B, Vrontinos S (1991) Classical formulation of the impact between bridge deck and abutments during strong earthquakes. In: Proceedings of the 6th Canadian conference on earthquake engineering, Toronto, Canada
Markogiannaki OG, Orologopoulos NG, Tegos IS (2017) Experimental and analytical study on hollow precast piers with unbonded conventional reinforcement to control seismic and in-service response of bridges. In: 6th ECCOMAS thematic conference on computational methods in structural dynamics and earthquake engineering, pp 282–296

Mashal M, Palermo A (2017) Experimental testing of emulative and post-tensioned earthquake damage resistant technologies for accelerated bridge construction. In: Proceedings of the 16th world conference on earthquake engineering, 16WCEE, Santiago, Chile

McKenna F, Fenves GL, Scott MH (2004) OpenSees: open system for earthquake engineering simulation. Pacific Earthquake Engineering Research Centre, University of California, Berkeley, CA. http://opensees.berkeley.edu. Accessed 18 Sept 2017

Moehle J, Deierlein GG (2004) A framework methodology for performance-based earthquake engineering. In: 13th world conference on earthquake engineering

Nielson BG, DesRoches R (2004) Improved methodology for generation of analytical fragility curves for highway bridges. In: 9th ASCE specialty conference on probabilistic mechanics and structural reliability, Albuquerque, NM, USA

O'Brien M, Saiidi M, Sadrossadat-Zadeh M (2007) A study of concrete bridge columns using innovative materials subjected to cyclic loading CCEER. Department of Civil Engineering, University of Nevada, Reno, Nevada, Report No. CCEER-07-01

Ozbulut OE, Hurlebaus S, Desroches R (2011) Seismic response control using shape memory alloys: a review. J Intell Mater Syst Struct 22:1531–1549

Padgett JE, DesRoches R (2007) Bridge functionality relationships for improved seismic risk assessment of transportation networks. Earthq Spectra 23:115–130

Padgett JE, DesRoches R (2008) Methodology for the development of analytical fragility curves for retrofitted bridges. Earthq Eng Struct Dyn 37:157–174

Padgett JE, DesRoches R, Ehlinger R (2010) Experimental response modification of a four-span bridge retrofit with shape memory alloys. Struct Control Health Monit 17:694–708

Palermo A, Pampanin S (2008) Enhanced seismic performance of hybrid bridge systems: comparison with traditional monolithic solutions. J Earthq Eng 12(8):1267–1295

Paulay T, Priestley MJN (1992) Seismic design of reinforced concrete and masonry buildings. Wiley, New York

PEER (Pacific Earthquake Engineering Research Center) (2013) PEER ground motion database. University of California, Berkeley, CA. http://ngawest2.berkeley.edu/. Accessed 18 Sept 2017

Porter KA (2003) An overview of PEER's performance-based earthquake engineering methodology. In: Proceedings of ninth international conference on applications of statistics and probability in civil engineering

Priestley MJN, Seible F, Calvi GM (1996) Seismic design and retrofit of bridges. Wiley, New York

Roh H, Reinhorn AM (2010) Hysteretic behavior of precast segmental bridge piers with superelastic shape memory alloy bars. Eng Struct 32:3394–3403

Saiidi MS, Wang H (2006) Exploratory study of seismic response of concrete columns with shape memory alloys reinforcement. ACI Struct J 103:435–442

Saiidi MS, O'Brien M, Sadrossadat-Zadeh M (2009) Cyclic response of concrete bridge columns using superelastic nitinol and bendable concrete. ACI Struct J 106(1):69–77

Scott BD, Park P, Priestley MJN (1982) Stress–strain behavior of concrete confined by overlapping hoops at low and high strain rates. J Am Concr Inst 79:13–27

Shinozuka M, Feng MQ, Kim H-K, Kim S-H (2000) Nonlinear static procedure for fragility curve development. J Eng Mech 126:1287–1295

Shrestha B, Hao H (2016) Parametric study of seismic performance of super-elastic shape memory alloy-reinforced bridge piers. Struct Infrastruct Eng 12:1076–1089

Su L, Wan HP, Dong Y, Frangopol DM, Ling XZ (2018) Efficient uncertainty quantification of wharf structures under seismic scenarios using Gaussian process surrogate model. J Earthq Eng 2018:1–22

Tremblay R, Lacerte M, Christopoulos C (2008) Seismic response of multistory buildings with self-centering energy dissipative steel braces. J Struct Eng 134:108–120

USGS (2017) Unified hazard tool. https://earthquake.usgs.gov/hazards/interactive/. Accessed 18 Sept 2017

Wang B, Zhu S (2018) Cyclic tension–compression behavior of superelastic shape memory alloy bars with buckling-restrained devices. Constr Build Mater 186:103–113

Wang W, Fang C, Liu J (2016) Self-centering beam-to-column connections with combined superelastic SMA bolts and steel angles. J Struct Eng 143(2):04016175

Wilde K, Gardoni P, Fujino Y (2000) Base isolation system with shape memory alloy device for elevated highway bridges. Eng Struct 22:222–229

Zhang J, Huo Y (2009) Evaluating effectiveness and optimum design of isolation devices for highway bridges using the fragility function method. Eng Struct 31:1648–1660

Zhang Y, Hu X, Zhu S (2009) Seismic performance of benchmark base-isolated bridges with superelastic Cu–Al–Be restraining damping device. Struct Control Health Monit 16(6):668–685

Zheng Y, Dong Y, Li Y (2018) Resilience and life-cycle performance of smart bridges with shape memory alloy (SMA)-cable-based bearings. Constr Build Mater 158:389–400